Materials International
Open-Access Journal (ISSN: 2668-5728)

Article
Volume 8, Issue 2, 2026, 12
https://doi.org/10.33263/Materials82.012

DFT Study of Evaluating the Potential of B_5N_{10}-Nanostructure Decorated with Al, C, and Si as the Smart Sensor for Hydrogen Detection

Fatemeh Mollaamin [1,*]

[1] Department of Biomedical Engineering, Faculty of Engineering and Architecture, Kastamonu University, Kastamonu, Turkey
* Correspondence: fmollaamin@kastamonu.edu.tr;

Received: 19.04.2025; Accepted: 27.07.2025; Published: 10.06.2026

Abstract: This study investigates the enhanced hydrogen gas adsorption on M (M = Al, C, and Si) doped boron nitride nanocage (BN) through first-principles density functional theory calculations. The results denote that H_2⟶ B_4MN_{10} are stable materials with the most stable adsorption spot being the heart of the cage cycle. The partial density of states can determine a specific charge transfer between H_2 and B_4MN_{10}. Analyzing NQR of C-based doping on B_5N_{10} has indicated the lowest fluctuation in electric potential and the highest negative charge distribution on doping atoms containing carbon, silicon, and aluminum in H_2⟶ B_4CN_{10}, H_2⟶ B_4SiN_{10}, and H_2⟶ B_4AlN_{10} heteroclusters, respectively. The reported results of NMR spectroscopy have exhibited that the yield of electron accepting for doping atoms on the B_4MN_{10} through H_2 adsorption can be categorized into Si≈Al>C, which displays the rigidity of the covalent bond between Al, C, Si, and H-atoms. Regarding IR spectroscopy, doped nanocages of H_2⟶ B_4SiN_{10} ≈, H_2⟶ B_4AlN_{10}>H_2⟶ B_4CN_{10}, respectively, have the most fluctuations and the highest adsorption tendency for hydrogen molecules, which can address specific questions on the individual effect of charge carriers, as well as doping atoms on the overall structure. Our findings provide important insights into the potential of employing B_4MN_{10} nanocages in hydrogen-based energy-storage approaches.

Keywords: H_2 adsorption; B_4AlN_{10}; B_4CN_{10} ; B_4SiN_{10}; battery cell; nanotechnology.

1. Introduction

Compared to traditional materials, boron nitride nanotubes (BNNTs) have a higher surface area, better structural and morphological characteristics, and greater activity. Hence, BNNTs are actively being investigated in a number of domains, including adsorption and gas adsorption applications. Boron nitride nanomaterials have been used owing to their unparalleled specifications of eco-friendly attributes for pollutant adsorption and semiconducting properties [1–4].

Boron nitride nanomaterials usually exhibit semi-leading behavior, which is considered a proper alternative to carbon nanotubes. The properties of boron and nitrogen atoms, which are the first neighbors of carbon in the periodic table, make boron nitride an interesting subject of numerous studies [5–7].

In recent years, various investigations on the adsorption of chemical contaminants and on the application of boron nitride nanostructures as adsorbents for water purification have been conducted [8–10].

Various physical shapes of boron nitride (BN)-based nano adsorbents such as nanoparticles, fullerenes, nanotubes, nanofibers, nanoribbons, nanosheets, nanomeshes, nanoflowers, and hollow spheres have been broadly considered possible adsorbents owing to their exceptional characteristics such as large surface area, structural variability, great chemical/mechanical strength, abundant structural defects, high reactive sites, and functional groups [11,12].

H_2 gas is mostly preserved either by liquefaction under high compressing pressure [13–16] or by adsorption on the surface or interstitial region of material cavity [17–19]. In this regard, the adsorption of H2 on the surfaces of 2D materials offers advantages in terms of safety, functionality, and cost-effectiveness. For the effective utilization of H_2 in fuel cells, the adsorption energy and gravimetric weight percentage on the adsorbent should be sufficiently high [20–24]. The adsorption-desorption kinetics and the strength of binding energy ought to be intermediate for hydrogen to bind on the material surfaces with an optimal adsorption energy range. Given the reasons mentioned above, we have explored the possibility of using boron nitride nanocages doped with aluminum, carbon, and silicon for H2 storage using first-principles calculations. We have analyzed the structural and electronic properties of M (M=Al, C, Si)–B_4N_{10} nanocages using state-of-the-art computational techniques [25–31].

Adsorption of charged adsorbates alters the double layer and the potential at the outer Helmholtz plane, thereby influencing the adsorption rates of both anodic and cathodic reactions. The first three modes are intimately associated with adsorption, and the double layer involves interaction of the adsorbates and the intermediate products. These compounds have been formed during partial electrochemical reactions and during the interaction of adsorbed intermediates with organic molecules, which can either inhibit or enhance the electrode reaction rate [32–49].

Against this backdrop, the current study focused on comparing various dopants (Al, C, and Si) and their effect on the B_5N_{10}'s adsorption ability towards H_2 using first-principle calculations. The effects of the doping of Al, C, and Si on the adsorption behavior of the B_5N_{10} have been investigated. The optimized geometries are used to analyze the geometrical parameters. The adsorption energies were measured in order to comprehend the thermodynamics of H_2 adsorption. The density of states, atomic charge, and electromagnetic properties were examined and verified using reactivity descriptors.

2. Materials and Methods

Theoretical approaches are a preliminary step and provide atomistic knowledge of interactions. Theoretical approaches are widely used in numerous investigations of BNNT-based materials for gas adsorption. The pristine BNNT exhibits a small surface area and is less sensitive to various gaseous molecules than its counterpart.

2.1. Hydrogen molecules adsorbed on B_4MN_{10}.

The aim of this study is to adsorb hydrogen molecules in the energy storage cell as an eco-friendly approach by using (Al, C, Si)-doped B_5N_{10} (Figure 1).

Boron nitride nanocage was modeled in the presence of doping atoms of aluminum, carbon, and silicon, which can increase the hydrogen sensing potential of BN-nanocage. In our research, sample characterization was performed by CAM–B3LYP–D3 /EPR–3, LANL2DZ level of theory.

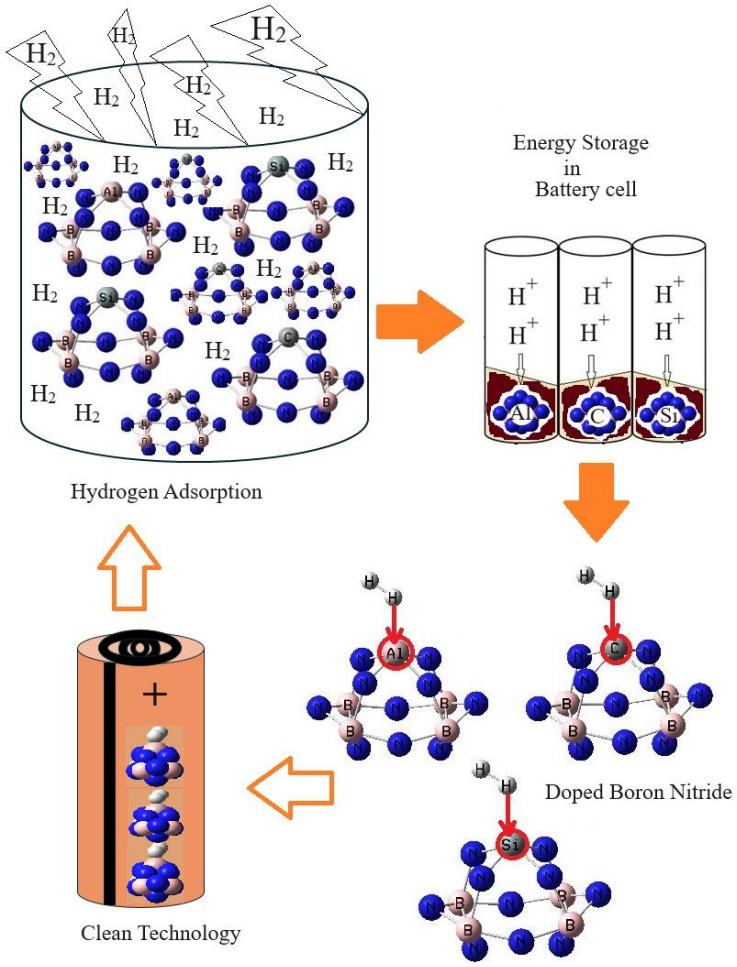

Figure 1. Application of B_4MN_{10} for adsorption of hydrogen molecules in the energy storage cell accompanying formation of complexes: H–H→ B_4AlN_{10}, H–H→ B_4CN_{10}, and H–H→ B_4SiN_{10}, complexes using CAM–B3LYP–D3/6-311+G (d,p), LANL2DZ calculation.

Figure 1 shows the process of adsorption of H_2 molecules on the B_4MN_{10} surface, which leads to the formation of complexes containing H–H→B_4AlN_{10}, H–H→B_4CN_{10}, and H–H→ B_4SiN_{10} complexes by molecular modeling computations.

The charge distribution of the mentioned complexes is calculated due to the Bader charge analysis [50]. The trapping of H_2 molecules by B_4MN_{10} (M =Al, C, Si) was successfully incorporated due to binding formation consisting of H→Al, H→C, and H→Si (Figure 1).

2.2. Application of the *density functional theory (DFT) approach.*

Hohenberg-Kohn (HK) functions have rigidly made the electronic density permissible as a fundamental variable for electronic and structure computations. In other words, the development of the applied DFT methodology only became notable after W. Kohn and L. J. Sham released their reputable series of equations, which are introduced as Kohn-Sham (KS) equations [51–58].

Considering the electronic density in the KS image points to a remarkable reduction in quantum computing. Thus, the KS methodology lightens the path to pursuing systems that

cannot be addressed by conventional ab initio methodologies. Kohn and Sham" introduces the solution which brings up the mono-electronic orbitals to account for the kinetic energy in a simple and relatively exact way, by finding a residual modification that might be computed apart. So, one starts with a reference model of *M* with non-interacting electrons related to the external potential v_s and with Hamiltonian [59–64]:

$$\hat{H}_s = -\sum_i^M \frac{1}{2} \overline{\nabla}_i^2 + \sum_i^M v_s(\vec{r}_i) = \sum_i^M \hat{h}_s \; ; \; \hat{h}_s = -\frac{1}{2} \overline{\nabla}_i^2 + v_s(\vec{r}_i) \quad (1)$$

By representing the single particle orbitals ψ_i all electronic densities physically acceptable for the system of "non-interacting" electrons are written in equation (2):

$$\rho(\vec{r}) = \sum_i^M |\psi_i(\vec{r})|^2 \quad (2)$$

Finally, the total energy could be measured by the KS method due to equation (3):

$$E[\rho] = \sum_i^M n_i \langle \psi_i \left| -\frac{1}{2} \overline{\nabla}^2 + v_{ext}(\vec{r}) + \frac{1}{2} \int \frac{\rho(\vec{r}')}{|\vec{r}-\vec{r}'|} \, d\vec{r}' \right| \psi_i \rangle + E_{xc}[\rho] + \frac{1}{2} \sum_\beta^N \sum_{\alpha \neq \beta}^N \frac{Z_\alpha Z_\beta}{|\vec{R}_\alpha - \vec{R}_\beta|} \quad (3)$$

Therefore, the precise exchange energy functional is described by the Kohn–Sham orbitals in lieu of the density, which is cited as the indirect density functional. This research has employed the penetration of the hybrid functional of the three-parameter basis set of B3LYP (Becke, Lee, Yang, Parr) within the conception of DFT upon theoretical computations [59–64]. The popular B3LYP (Becke, three-parameter, Lee–Yang–Parr) and exchange-correlation functional becomes based on equation (4) [59–64]:

$$E_{\mathrm{XC}}^{\mathrm{B3LYP}} = (1-\alpha) E_{\mathrm{x}}^{\mathrm{LSDA}} + \alpha E_{\mathrm{x}}^{\mathrm{HF}} + b \Delta E_{\mathrm{x}}^{\mathrm{B}} + (1-c) E_{\mathrm{c}}^{\mathrm{LSDA}} + c E_{\mathrm{c}}^{\mathrm{LYP}} \quad (4)$$

$\alpha = 0.20, b = 0.72, c = 0.81$ shows a generalized gradient approximation: the Becke exchange functional [57] and the correlation functional of Lee, Yang, and Parr [58] for B3LYP and $E_{\mathrm{c}}^{\mathrm{LSDA}}$ is the VWN local spin density approximation to the correlation functional [59].

In this article, the rigid PES using DFT calculations has been computed applying Gaussian 16 revision C.01 software [65]. The input Z-matrix for the adsorption of H_2 molecules by the B_4MN_{10} has been designed with GaussView 6.1 [66] using 6-311+G (d,p), EPR–3, LANL2DZ basis set. In this study, the interaction between H_2 molecules and B_4MN_{10} was modeled and analyzed. As revealed by DFT-based analysis, the potency of B_4MN_{10} for grabbing H_2 molecules was determined mainly by the electronegativity of the functional groups, as well as the interaction between the B_4MN_{10} and the H_2 molecules [67,68].

2.3. Nuclear quadrupole resonance (NQR).

The NQR method is related to the multipole expansion in Cartesian coordinates as in equation (5) [69,70]:

$$V(r) = V(0) + \left[\left(\frac{\partial V}{\partial x_i} \right) \Big|_0 . \partial x_i \right] + \frac{1}{2} \left[\left(\frac{\partial^2 V}{\partial x_i x_j} \right) \Big|_0 . \partial x_i \partial x_j \right] \quad (5)$$

After that, a simplification of the equation (5), there are only the second derivatives related to the identical variable for the potential energy [38,39]:

$$U = -\frac{1}{2} \int_{\mathcal{D}} d^3 r \, \rho_r \left[\left(\frac{\partial^2 V}{\partial x_i^2} \right) \Big|_0 . \partial x_i^2 \right] = -\frac{1}{2} \int_{\mathcal{D}} d^3 r \, \rho_r \left[\left(\frac{\partial E_i}{\partial x_i} \right) \Big|_0 . \partial x_i^2 \right] = -\frac{1}{2} \left(\frac{\partial E_i}{\partial x_i} \right) \Big|_0 . \int_{\mathcal{D}} d^3 r \, [\rho(r) . \partial x_i^2] \quad (6)$$

There are two parameters which must be obtained from NQR experiments: the quadrupole coupling constant, χ, and the asymmetry parameter of the EFG tensor, η:

$$\chi = {}^{e^2 Q q_{zz}}/_{h} \quad (7)$$

$$\eta = {}^{q_{xx} - q_{yy}}/_{q_{zz}} \qquad (8)$$

where q_{ii} are ingredients of the EFG tensor at the quadrupole nucleus are determined in the EFG principal axes system, Q is the nuclear quadrupole moment, e is the proton charge, and h is Planck's constant [69,70].

3. Results and Discussion

In this article, the efficiency of boron nitride nanocage doped with aluminum, carbon, and silicon (B_4MN_{10}) for hydrogen detection is discussed. In fact, it can be remarked that the chemisorptive nature of the bond among the hydrogen molecules with boron and nitrogen elements through the equilibrium distribution of doping atoms, B_5N_{10}, and a monolayer attribute.

3.1. PDOS and electronic evaluation.

The electronic structures of hydrogen adsorption on the M (Al, C, Si)–doped B_5N_{10} as the smart molecule sensor have been illustrated using CAM–B3LYP–D3/6-311+G (d,p), LANL2DZ level of theory.

Figure 2 (a–c) shows the projected density of state (PDOS) of H_2→ (Al, C, Si)–B_4N_{10} through hydrogen molecule adsorption. The appearance of the energy states (*p*-orbital) of Al, C, Si, and N within the gap of (Al, C, and Si)–B_4N_{10} induces the reactivity of the system.

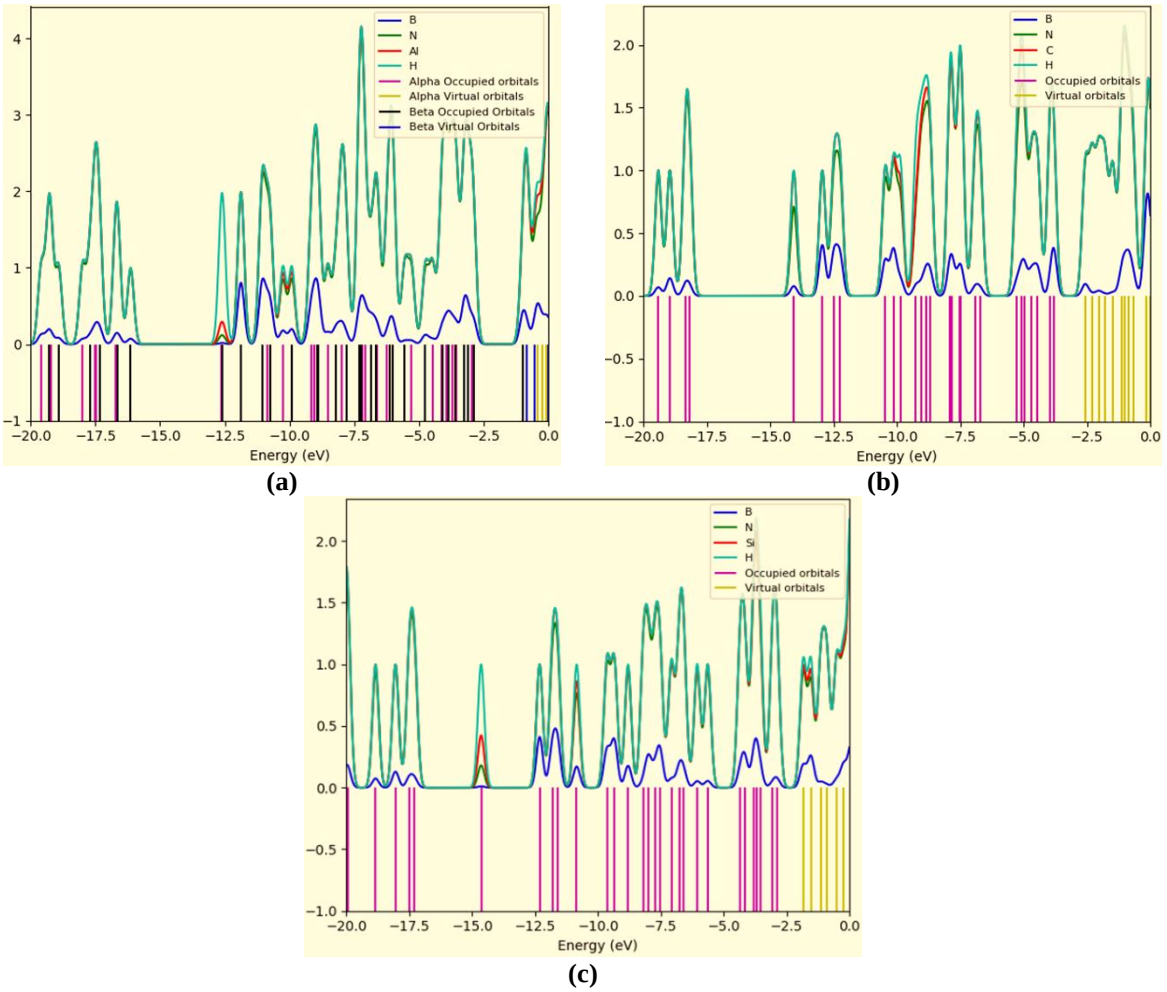

Figure 2. PDOS of H_2 adsorbed on B_4MN_{10} including **(a)** H_2→ B_4AlN_{10}; **(b)** H_2→ B_4CN_{10}; **(c)** H_2→ B_4SiN_{10} complexes by CAM–B3LYP–D3/6–311+G (d,p), LANL2DZ.

It is clear from the figure that after trapping with hydrogen molecules, there is a significant contribution of the *p*-orbital in the unoccupied level. Therefore, the curve of partial PDOS describes that the *s* states of H atoms and Al, C, and Si atoms in B_4MN_{10} are overcome due to the conduction band (Figure 2a–c). A distinguished adsorption trait might be seen in $H_2 \rightarrow B_4MN_{10}$ because of the potent interaction between the *s* states of hydrogen atoms with *p* states of Al, C, and Si in B_4MN_{10} complexes.

Figure 2(a–c) shows that $H_2 \rightarrow B_4AlN_{10}$, $H_2 \rightarrow B_4CN_{10}$, and $H_2 \rightarrow B_4SiN_{10}$ complexes through hydrogen adsorption, respectively, have the most contribution at the middle of the conduction band between –5 to –10 eV, while contribution of boron and nitrogen states are enlarged and similar together, and adsorbing of H_2 depicts interfacial electronic of the B_4N_{10} for selection of hydrogen molecules. $H_2 \rightarrow B_4AlN_{10}$ has indicated sharp peaks for the Al atom close to H atoms in Figure 2 (a). $H_2 \rightarrow B_4CN_{10}$ (Figure 2 b) has exhibited strong peaks for the C atom close to the H atoms. Furthermore, the sharp Si graph near H atoms in $H_2 \rightarrow B_4SiN_{10}$ (Figure 2c) has been indicated. Therefore, the order ability of hydrogen adsorption by doping atoms of Al, C, and Si on B_4MN_{10} based on the PDOS might be shifted as: $B_4SiN_{10} > B_4CN_{10} > B_4AlN_{10}$.

3.2. Insight into electric potential analysis.

As the electric field gradient (EFG) at the citation of the nucleus in H_2 is allocated by the valence electrons twisted in the attachment with close nuclei of B_4MN_{10} (M =Al, C, and Si) through trapping of hydrogen molecules, the NQR frequency at which transitions occur is particular for $H_2 \rightarrow$ (Al, C, and Si)–B_4N_{10} complexes (Table1).

In this research work, the electric potential as the quantity of work energy through carrying over the electric charge from one position to another position in the essence of the electric field has been evaluated for $H_2 \rightarrow B_4AlN_{10}$, $H_2 \rightarrow B_4CN_{10}$, and $H_2 \rightarrow B_4SiN_{10}$ complexes (Table 1).

Table1. The electric potential (a.u.) and Bader charge (coulomb) through NQR calculation for $H_2 \rightarrow B_4AlN_{10}$, $H_2 \rightarrow B_4CN_{10}$, and $H_2 \rightarrow B_4SiN_{10}$ complexes using CAM–B3LYP–D3/EPR–3, LANL2DZ calculation.

H–H→ B_4AlN_{10}			**H–H → B_4CN_{10}**			**H–H → B_4SiN_{10}**		
Atom	**Q**	**E_p**	**Atom**	**Q**	**E_p**	**Atom**	**Q**	**E_p**
B1	0.28	–11.31	B1	0.29	–11.27	B1	0.32	–11.27
N2	–0.18	–18.15	N2	–0.15	–18.09	N2	–0.16	–18.12
N3	–0.11	–18.12	N3	–0.14	–18.07	N3	–0.16	–18.12
B4	0.28	–11.31	B4	0.29	–11.26	B4	0.32	–11.28
B5	0.30	–11.30	B5	0.29	–11.27	B5	0.32	–11.28
B6	0.31	–11.29	B6	0.29	–11.27	B6	0.33	–11.28
N7	–0.17	–18.14	N7	–0.15	–18.09	N7	–0.16	–18.13
N8	–0.15	–18.14	N8	–0.13	–18.08	N8	–0.15	–18.10
N9	–0.36	–18.21	N9	–0.10	–18.09	N9	–0.34	–18.18
N10	–0.37	–18.21	N10	–0.10	–18.09	N10	–0.35	–18.18
N11	–0.33	–18.20	N11	–0.09	–18.08	N11	–0.33	–18.17
N12	–0.36	–18.19	N12	–0.10	–18.07	N12	–0.34	–18.17
Al13	1.15	–43.68	C13	0.11	–14.52	Si13	1.06	–48.33
N14	–0.16	–18.12	N14	–0.14	–18.08	N14	–0.19	–18.13
N15	–0.17	–18.14	N15	–0.14	–18.08	N15	–0.18	–18.13
H16	–0.03	–1.06	H16	0.02	–1.17	H16	–0.02	–1.01
H17	0.09	–1.02	H17	–0.02	–1.21	H17	0.04	–1.10

In Table 1, the Bader charge and electronic potential properties of Al, C, and Si–B, N in B_4MN_{10} and hydrogen molecules absorbed on atom–doped boron nitride nanocage have been investigated. The amounts indicate that with increasing the negative charge of different

atoms, the electric potential resulting from NQR calculations increases. Moreover, the doping atoms of Al (13), C (1), and Si (13) on the B_4N_{10} have shown the most potential for accepting the electron from the electron donor of H (16) and H (17) in H_2 adsorbed on the B_4N_{10} (Table 1).

Furthermore, in Figure 3 (a–c), the electric potential of nuclear quadrupole resonance for some atoms of Al, C, and Si/B, N in B_4MN_{10} and H atoms of H_2 molecule trapped on atom–doped boron nitride nanocage, which has been calculated by CAM–B3LYP–D3/EPR–3, LANL2DZ.

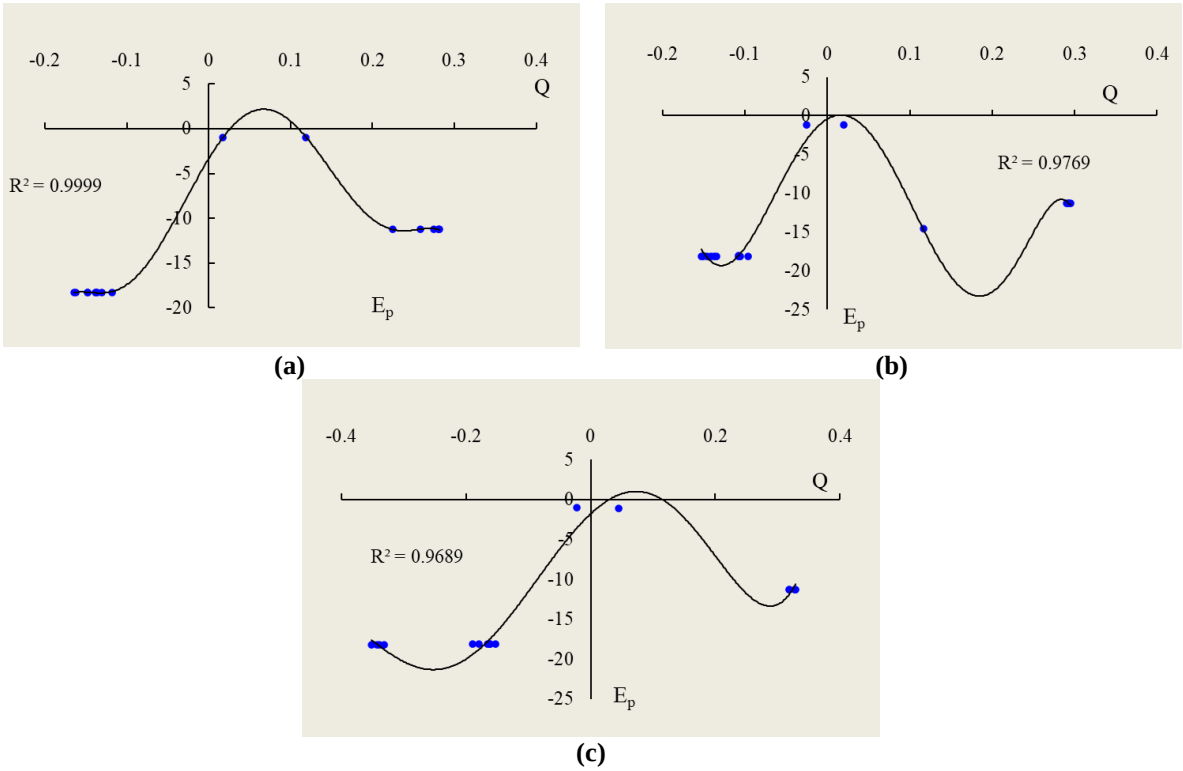

Figure 3. Electric potential (a.u.) versus Bader charge (coulomb) through NQR calculation for **(a)** H–H→ B_4AlN_{10}; **(b)** H–H → B_4CN_{10}; **(c)** H–H → B_4SiN_{10} complexes by CAM–B3LYP–D3/EPR–3, LANL2DZ.

In Figure 3 (a), the behavior of H_2 adsorption on the B_4AlN_{10} was observed with high sensitivity based on the relation coefficient of $R^2 = 0.9276$. Adsorption of H_2 on the B_4CN_{10} and in Figure 3 (b) has illustrated the highest sensing of $R^2 = 0.9769$. In addition, Figure 3 (c) shows that B_4SiN_{10} has a good detection for H_2 adsorption in the battery cell based on the relation coefficient of $R^2 = 0.9689$.

It's vivid that the curve of B_4MN_{10} is wavy due to these H_2 molecules. The fluctuated peaks for electric potential have been shown around H_2 trapping on the B_4MN_{10}, which demonstrates the electron accepting specifications of hydrogen versus the aluminum, carbon, and silicon doped on the B_5N_{10} (Figure 3a–c). Besides, it can be considered that carbon (Figure 3b) and silicon (Figure 3c) are semiconductor elements in the functionalized B4N10, which might exhibit greater sensitivity to accepting electrons from H atoms during adsorption. However, aluminum-doped on B_5N_{10} (adsorbent) has shown the lowest fluctuation (R^2 = 0.9276) between Bader charge versus electric potential extracted from NQR parameters and the lowest negative atomic charge including 1.1541 coulomb in H_2→ B_4AlN_{10} which can be an appropriate option for H_2 molecules (adsorbate) after B_4CN_{10} with 0.1167 coulomb on C atom and B_4SiN_{10} with 1.0620 coulomb on Si atom, the highest tendency for electron accepting in the adsorption current (Table 1).

In fact, the uptake of H_2 molecules has been shown to be associated with B4MN10, indicating that the adsorbed hydrogen molecules in the Mdoped nanocage can be internalized via a different pathway than in the pristine nanocage.

3.3. Nuclear magnetic resonance spectra.

Based on the resulting amounts, nuclear magnetic resonance (NMR) spectra of M (Al, C, and Si)–B_4N_{10} complexes can be used as a potent sensor for adsorbing H_2 molecules, thereby unraveling the efficiency of B_4MN_{10} for saving clean energy as an eco-friendly approach in battery cells.

From the DFT calculations, the chemical shielding (CS) tensors in the principal axes system to estimate the isotropic chemical shielding (CSI) and anisotropic chemical shielding (CSA) [71]:

$$\sigma_{iso} = (\sigma_{11} + \sigma_{22} + \sigma_{33})/3 \quad (9)$$

$$\sigma_{aniso} = \sigma_{33} - (\sigma_{22} + \sigma_{11})/2 \quad (10)$$

The NMR data of isotropic (σ_{iso}) and anisotropic shielding tensors (σ_{aniso}) of hydrogen molecules trapped in the B_4MN_{10} towards formation of H_2→ B_4AlN_{10}, H_2→ B_4CN_{10}, and H_2→ B_4SiN_{10} complexes have been computed by the Gaussian 16 revision C.01 program package [65] and are shown in Table 2.

Table 2. Data of NMR shielding tensors for selected atoms of H_2⟶ B_4AlN_{10}, H_2⟶ B_4CN_{10}, and H_2⟶ B_4SiN_{10} complexes using CAM–B3LYP–D3/6-311+G (d,p), LANL2DZ calculation.

H–H⟶ B_4AlN_{10}			**H–H ⟶ B_4CN_{10}**			**H–H ⟶ B_4SiN_{10}**		
Atom	**σ_{iso}**	**σ_{aniso}**	**Atom**	**σ_{iso}**	**σ_{aniso}**	**Atom**	**σ_{iso}**	**σ_{aniso}**
B1	97.53	83.40	B1	104.44	91.68	B1	75.38	57.49
N2	256.12	636.67	N2	122.34	619.504	N2	33.56	576.41
N3	62.43	79.19	N3	1555.43	2736.94	N3	1098.19	2362.50
B4	105.73	72.88	B4	100.08	126.13	B4	104.48	42.51
B5	95.50	55.88	B5	126.13	40.37	B5	60.95	54.51
B6	78.10	73.12	B6	110.96	62.81	B6	56.07	69.73
N7	173.56	565.37	N7	248.31	382.14	N7	49.56	1405.12
N8	78.65	254.42	N8	516.69	1188.98	N8	1110.12	1984.65
N9	472.62	831.22	N9	593.24	1206.16	N9	18.26	5065.21
N10	569.41	703.54	N10	871.58	1747.50	N10	528.91	2567.90
N11	508.15	940.57	N11	1075.36	1808.54	N11	446.94	4452.66
N12	275.13	706.00	N12	601.11	1086.02	N12	146.36	1615.65
Al13	522.13	157.54	C13	106.50	79.78	Si13	722.90	178.47
N14	26.41	596.76	N14	0.53	1401.62	N14	253.75	706.94
N15	18.66	593.71	N15	268.24	1157.89	N15	46.21	1894.76
H16	23.45	2.75	H16	24.29	6.76	H16	16.54	32.84
H17	21.29	2.81	H17	26.55	3.36	H17	22.67	25.85

In Table 2, NMR data have reported notable amounts for H_2 molecules, which were adsorbed on the B_4MN_{10} as a selective sensor for saving energy. The observed increase in the chemical shift anisotropies spans for H atoms adsorption on the B_4MN_{10} are near N(9), N(10), N(11), N(12), N(14), and N(15). The observed weak signal intensity near the parallel edge of the nanocage pattern may be due to boron binding-induced non-spherical distribution of these complexes.

It is remarkable that doping of Al, C, and Si on B_5N_{10} might promote the stability of the nanocage that results in enhanced magnetic alignment of complexes. Interestingly, the

reported results show that Al, C, and Si elements can be optimized to achieve optimal alignment of the nanocage in the presence of an applied magnetic field.

In fact, the adsorption of H_2 can introduce spin polarization on the B_4MN_{10}, which indicates that these surfaces might be applied as a magnetic scavenging surface as a hydrogen detector. Isotropic and anisotropic shielding fluctuate with the occupancy in the electron-accepting hydrogen molecules trapped in the atom-doped on the boron nitride nanocage.

Figure 4 (a–c) exhibited the same tendency of shielding for boron and nitrogen; however, a considerable deviation exists from doping atoms of Al(13), C(13), and Si(13) through interaction with H(16) of H_2 molecules during adsorption on the B_5N_{10}.

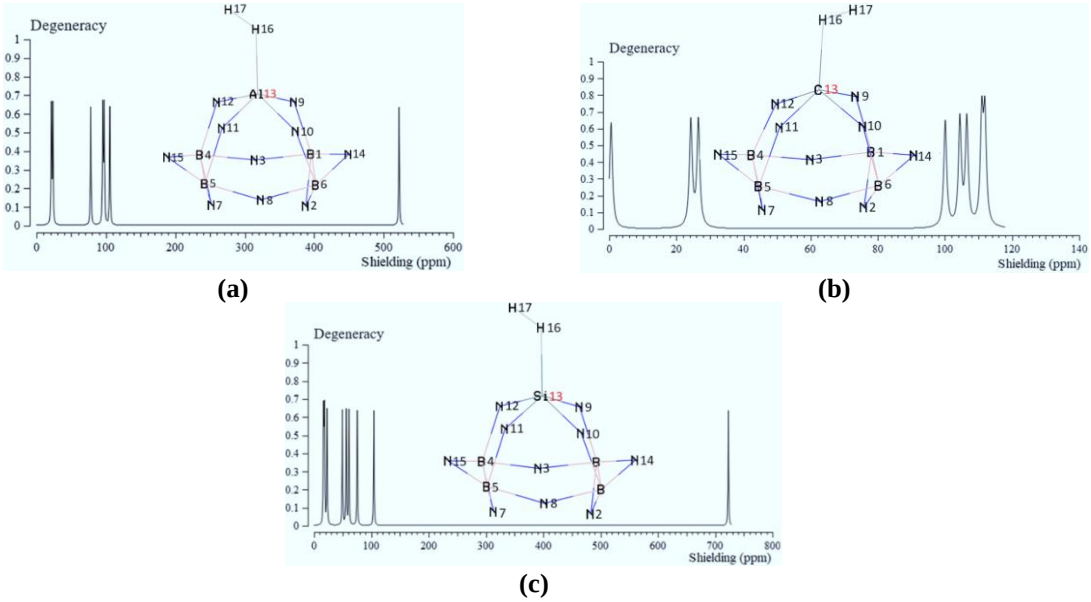

Figure 4. The NMR spectra for **(a)** $H_2 \rightarrow B_4AlN_{10}$; **(b)** $H_2 \rightarrow B_4CN_{10}$; **(c)** $H_2 \rightarrow B_4SiN_{10}$ complexes using CAM–B3LYP–D3/6–311+G (d,p), LANL2DZ.

In Figure 4 (a–c), H_2 molecules in the complexes of $H_2 \rightarrow B_4AlN_{10}$ (Figure 4a), $H_2 \rightarrow B_4CN_{10}$ (Figure 4b), and $H_2 \rightarrow B_4SiN_{10}$ (Figure 4c) denote the fluctuation in the chemical shielding during ion trapping.

Figure 4 (a–c) shows the gap chemical shielding between aluminum, carbon, silicon and hydrogen molecules in B_4MN_{10} complexes. The yield of electron acceptors for doping atoms on the B_4MN_{10} complexes through hydrogen molecule adsorption can be ordered as: Si≈Al>C, which supports the possibility of a covalent bond between aluminum, carbon, silicon, and hydrogen atoms in H_2 molecules towards energy storage in battery technology.

In NMR spectroscopy, it has been observed that the prominent peaks around the interaction of H2 molecules with adsorbed B_4MN_{10} during molecule detection; however, there are fluctuations in the chemical shielding behavior, both isotropic and anisotropic.

Therefore, the authors believe that the extracted results would be useful for the design of B_4MN_{10}-doped nanomaterials to enhance hydrogen adsorption, as well as for structural studies using solid-state and solution NMR techniques.

3.4. Infrared (IR) spectroscopy and thermodynamic factors.

The IR calculations have been accomplished for the adsorption of H_2 molecules by B_4MN_{10} during hydrogen sensing. Therefore, it has been simulated the several clusters containing $H_2 \rightarrow B_4AlN_{10}$ (Figure 5a), $H_2 \rightarrow B_4CN_{10}$ (Figure5b), and $H_2 \rightarrow B_4SiN_{10}$ (Figure 5c) using CAM–B3LYP–D3/6-311+G (d,p), LANL2DZ.

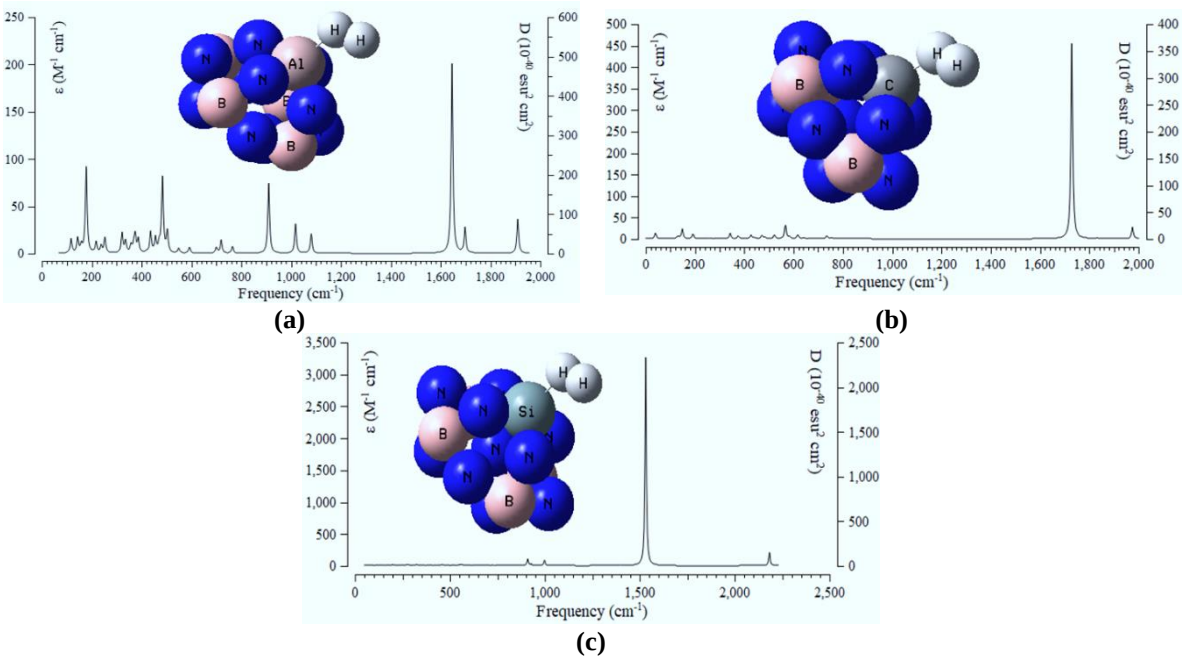

Figure 5. The Frequency (cm^{-1}) changes through the IR spectra for **(a)** $H_2 \rightarrow B_4AlN_{10}$; **(b)** $H_2 \rightarrow B_4CN_{10}$; **(c)** $H_2 \rightarrow B_4SiN_{10}$ complexes using CAM–B3LYP–D3/6-311+G (d,p), LANL2DZ.

The graph of Figure 5 (a) has been observed in the frequency range between 100–2000 cm^{-1} for $H_2 \rightarrow B_4AlN_{10}$ with several sharp peaks around 177.92, 483.81, 910.24, and 1645.95 cm^{-1}. Figure 5 (b) shows the frequency range between 200–2000 cm^{-1} for $H_2 \rightarrow B_4CN_{10}$ with a sharp peak around 1729.19 cm^{-1}. Figure 5 (c) indicates the fluctuation of frequency between 1000–2500 cm^{-1} for $H_2 \rightarrow B_4AlN_{10}$ with a sharp peak around 1531.05 cm^{-1}.

The IR spectra of H_2 adsorption with B_4MN_{10} have demonstrated that the structure of the dominant complex correlates with the electron potency of doped M (Al, C, Si) on the B_5N_{10}. The doped nanocage of B_4AlN_{10} (Figure 5a) has shown the most fluctuations and the highest tendency for adsorption of H_2 molecules than B_4CN_{10} and B_4SiN_{10} complexes, respectively (Figure 5b and c). Therefore, it can be found that IR spectroscopy of H_2-adsorbed B_4AlN_{10} is now well-placed to address specific questions on the individual effect of charge carriers (hydrogen molecule-nanocage), as well as doping atoms on the overall structure (Figure 5a–c).

Table 3, through the thermodynamic specifications, concluded that M (Al, C, Si)–B_4N_{10}, due to the adsorption of H_2, might be more efficient sensors for detecting and absorbing the hydrogen molecules towards the energy storage in battery cells and its implications for clean energy technology.

Table 3. The thermodynamic characters of $H_2 \rightarrow B_4AlN_{10}$, $H_2 \rightarrow B_4CN_{10}$ and $H_2 \rightarrow B_4SiN_{10}$ complexes using CAM–B3LYP–D3/6-311+G (d,p), LANL2DZ calculation.

Compound	$\Delta E^o_{ads} \times 10^{-3}$ (kcal/mol)	$\Delta H^o_{ads} \times 10^{-3}$ (kcal/mol)	$\Delta G^o_{ads} \times 10^{-3}$ (kcal/mol)	S^o_{ads} (cal/K.mol)	Dipole moment (Debye)
B_5N_{10}	–420.550	–420.549	–420.579	100.650	0.202
B_4AlN_{10}	–406.553	–406.553	–406.584	105.620	3.946
B_4CN_{10}	–428.953	–428.952	–428.982	99.184	1.759
B_4SiN_{10}	–407.701	–407.700	–407.730	102.387	1.266
$H_2 \rightarrow B_4AlN_{10}$	–551.051	–551.050	–551.081	104.003	4.403
$H_2 \rightarrow B_4CN_{10}$	–424.231	–424.231	–424.260	99.710	1.472
$H_2 \rightarrow B_4SiN_{10}$	–580.207	–580.206	–580.235	95.419	2.812

Thermodynamic parameters of H_2 molecules' adsorption on the B_4MN_{10} complexes have been determined using the DFT theoretical technique. It has been shown that for a given number of hydrogen donor sites in H_2 molecules, the stabilities of complexes owing to doping

atoms of Al, C, and Si can be considered as: H_2→ B_4SiN_{10}>H_2→ B_4AlN_{10}>>>H_2→ B_4CN_{10} complexes (Table 3). The changes of Gibbs free energy versus dipole moment in Figure 6 could detect the maximum efficiency of Al, C, and Si atoms doping of B_4N_{10}_NC for H_2 molecules adsorption through ΔG^o_{ads} which depends on the covalent bond between H_2 molecules and B_4MN_{10} as a potent sensor for air pollution removal.

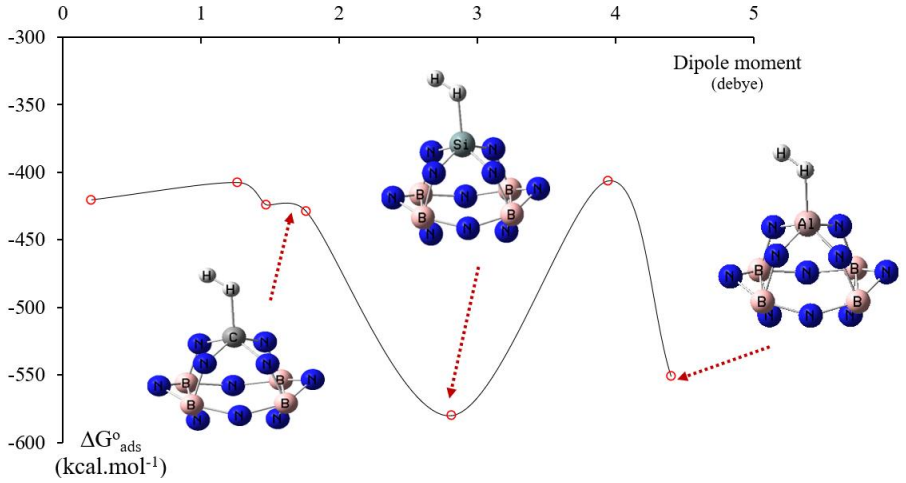

Figure 6. Gibbs free energy (ΔG^o_R) for H_2→ B_4AlN_{10}, H_2→ B_4CN_{10}, and H_2→ B_4SiN_{10} complexes using CAM–B3LYP–D3/6-311+G (d,p), LANL2DZ calculation.

The adsorption process of H_2 molecules on the B_4MN_{10} is affirmed by the ΔG^o_{ads} quantities:

$$\Delta G^o_{ads} = \Delta G^o_{H2\rightarrow B4MN10} - (\Delta G^o_{H2} + \Delta G^o_{B4MN10}) \text{ , M = Al, C, Si} \quad (11)$$

Figure 6 shows the key role of doped atoms containing Al, C, and Si during interaction between the adsorbate of H_2 molecules as the electron donors and the adsorbent of B_4AlN_{10}, B_4CN_{10}, and B_4SiN_{10} nanocages as electron acceptors. Therefore, the selectivity of atom-doping on boron nitride nanocage (hydrogen sensor) for H_2 adsorption can be expressed as: Si>Al>>>C (Table 3 and Figure 6).

By combining experimental data with first-principles calculations, the interaction mechanism between the BN nanocage and H_2 molecules is identified as physical adsorption, and the doped atoms can enhance polarization and magnify the binding energy [72].

4. Conclusions

This research has investigated doping of M (Al, C, Si) elements on the boron nitride (B_5N_{10}) nanocage for enhancing H_2 sensing, applying it in the hydrogen-based energy storage technology. Therefore, H_2 molecule adsorption on B_4MN_{10} nanocages has been investigated based on electrostatic interactions between the H_2 molecules and the B_4MN_{10} complexes. The electromagnetic and thermodynamic properties of B_4MN_{10} complexes were computed using density functional theory. The results have illustrated that chosen hydrogen molecules adsorbed on the B_4MN_{10} are rather stable, with the most stable adsorption site being in the center of the B_4MN_{10} system. The selectivity of atom-doping on boron nitride nanocage (hydrogen sensor) for H_2 molecules adsorption can be expressed as: H_2→ B_4SiN_{10}>H_2→ B_4AlN_{10}>>>H_2→ B_4CN_{10} complexes, respectively. This work proposes that metallic, nonmetallic, and metalloid semiconductors can be examined by doping nanomaterials to enhance adsorption potency for designing pollution-removal sensors.

Author Contributions

Conceptualization, F.M.; methodology, F.M.; software, F.M.; validation, F.M.; formal analysis, F.M.; investigation, F.M.; data curation, F.M.; writing—original draft preparation, F.M.; writing—review and editing, F.M.; visualization, F.M.; All authors have read and agreed to the published version of the manuscript.

Institutional Review Board Statement

Not applicable.

Informed Consent Statement

Not applicable.

Data Availability Statement

Not applicable.

Funding

This research received no external funding.

Acknowledgments

The author is grateful to Kastamonu University for successfully completing this paper and its research.

Conflict of Interest

The author declares no conflict of interest.

References

1. Ran, H.; Yin, J.; Li, H. Editorial for the Special Issue on "Boron Nitride-Based Nanomaterials". *Nanomaterials* **2023**, *13*, 584, https://doi.org/10.3390/nano13030584.
2. Shtansky, D.V.; Matveev, A.T.; Permyakova, E.S.; et al., Recent Progress in Fabrication and Application of BN Nanostructures and BN-Based Nanohybrids. *Nanomaterials* **2022**, *12*, 2810, https://doi.org/10.3390/nano12162810.
3. Alengebawy, A.; Abdelkhalek, S.T.; Qureshi, S.R.; Wang, M.-Q. Heavy Metals and Pesticides Toxicity in Agricultural Soil and Plants: Ecological Risks and Human Health Implications. *Toxics* **2021**, *9*, 42, https://doi.org/10.3390/toxics9030042.
4. Mollaamin, F.; Monajjemi, M. Trapping of toxic heavy metals from water by GN–nanocage: Application of nanomaterials for contaminant removal technique. *J. Mol. Struct.* **2024**, *1300*, 137214, https://doi.org/10.1016/j.molstruc.2023.137214.
5. Mollaamin, F.; Monajjemi, M. Nanomaterials for Sustainable Energy in Hydrogen-Fuel Cell: Functionalization and Characterization of Carbon Nano-Semiconductors with Silicon, Germanium, Tin or Lead through Density Functional Theory Study. *Russ. J. Phys. Chem. B.* **2024**, *18*, 607–623, https://doi.org/10.1134/S1990793124020271.
6. Mollaamin, F.; Monajjemi, M. The influence of Sc, V, Cr, Co, Cu, Zn as ferromagnetic semiconductors implanted on B_5N_{10}-nanocarrier for enhancing of NO sensing: An environmental eco-friendly investigation. *Comput. Theor. Chem.* **2024**, *1237*, 114666, https://doi.org/10.1016/j.comptc.2024.114666.

7. Halleb, A.; Yokoyama, F.; das Neves, M.A.; Nakajima, M. Effects of surfactants and oil-in-water emulsions on reverse osmosis membrane performance. *Euro-Mediterr. J. Environ. Integr.* **2021**, *6*, 44, https://doi.org/10.1007/s41207-020-00236-1.
8. Cheng, Y.; Xue, F.; Yu, S.; Du, S.; Yang, Y. Subcritical Water Extraction of Natural Products. *Molecules* **2021**, *26*, 4004, https://doi.org/10.3390/molecules26134004.
9. Mollaamin, F. Competitive Intracellular Hydrogen-Nanocarrier Among Aluminum, Carbon, or Silicon Implantation: a Novel Technology of Eco-Friendly Energy Storage using Research Density Functional Theory. *Russ. J. Phys. Chem. B.* **2024**, *18*, 805–820, https://doi.org/10.1134/S1990793124700131.
10. Mollaamin, F.; Shahriari, S.; Monajjemi, M. Influence of Transition Metals for Emergence of Energy Storage in Fuel Cells through Hydrogen Adsorption on the MgAl Surface. *Russ. J. Phys. Chem. B* **2024**, *18*, 398–418, https://doi.org/10.1134/S199079312402026X.
11. Dokhlikova, N.; Ozerin, S.; Doronin, S.; Rudenko, E.; Grishin, M.; Shub, B. Simulation of Hydrogen and Oxygen Adsorption on Nickel and Platinum Nanoparticles Located on a Graphite Substrate with Various Defects. *Russ. J. Phys. Chem. B* **2022**, *16*, 461-467, https://doi.org/10.1134/S1990793122030137.
12. Monajjemi, M.; Mohammadi, S.; Shahriari, S.; Mollaamin, F. Experimental and Theoretical Studies of ZnO Nanotubes: an Approach to Chemical Physics Characterization of ZnONTs, Including Morphology, Piezoelectric, and Density of States. *Russ. J. Phys. Chem. B.* **2024**, *18*, 308–324, https://doi.org/10.1134/S1990793124010342.
13. Hiratsuka,A.; Yasuda, Y. Study on the Possibility of Mixed Water as a Drinking Water—From the Viewpoint of the Formation of Hydrogen-Rich Water. *J. Water Resour. Prot.* **2021**, *13*, 44–73, https://doi.org/10.4236/jwarp.2021.131004.
14. Marszałek, J.; Żyłła, R. Recovery of Water from Textile Dyeing Using Membrane Filtration Processes. *Processes* **2021**, *9*, 1833, https://doi.org/10.3390/pr9101833.
15. Dogra, V.; Kaur, G.; Kumar, R.; Kumar, S. Toxicity Profiling of Metallosurfactant Based Ruthenium and Ruthenium Oxide Nanoparticles towards the Eukaryotic Model Organism Saccharomyces Cerevisiae. *Chemosphere* **2021**, *270*, 128650, https://doi.org/10.1016/j.chemosphere.2020.128650.
16. Góralczyk-Bińkowska, A.; Długoński, A.; Bernat, P.; Długoński, J.; Jasińska, A. Environmental and molecular approach to dye industry waste degradation by the ascomycete fungus Nectriella pironii. *Sci. Rep.* **2021**, *11*, 23829, https://doi.org/10.1038/s41598-021-03446-x.
17. Wang, Y.; Yi, Q.; Ding, Y.; Ji, F.; Wang, N. Study on the Factors Influencing the Dyeing Performance of Cotton Fabric with Vat Dyes Based on Principal Component Analysis. *J. Text. Inst.* **2021**, *112*, 1460–1466, https://doi.org/10.1080/00405000.2020.1824432.
18. Sewu, D.D.; Lee, D.S.; Woo, S.H.; Kalderis, D. Decolorization of Triarylmethane Dyes, Malachite Green, and Crystal Violet, by Sewage Sludge Biochar: Isotherm, Kinetics, and Adsorption Mechanism Comparison. *Korean J. Chem. Eng.* **2021**, *38*, 531–539, https://doi.org/10.1007/s11814-020-0727-7.
19. Singh, J.; Gupta, P.; Das, A. Dyes from Textile Industry Wastewater as Emerging Contaminants in Agricultural Fields. In Sustainable Agriculture Reviews 50: Emerging Contaminants in Agriculture, Kumar Singh, V., Singh, R., Lichtfouse, E., Eds.; Springer International Publishing: Cham, **2021**; pp. 109-129, https://doi.org/10.1007/978-3-030-63249-6_5.
20. Mollaamin, F.; Monajjemi, M. Boron nitride doped with transition metals for carbon monoxide detection: a promising nanosensor for air cleaning. *Sensor Rev.* **2024**, *44*, 179–193, https://doi.org/10.1108/SR-01-2024-0066.
21. Kozlov, S.N.; Zhestkov, B.E. Effect of the Composition of a Gas Mixture on Determining the Probability of Heterogeneous Recombination of H, O, and N Atoms on Quartz. *Russ. J. Phys. Chem. B.* **2022**, *16*, 1030–1037, https://doi.org/10.1134/S1990793122060069.
22. Kuperman, A.; Sergeev, A.Y.; Turusov, R.; Solodilov, V. Influence of a Sealing Layer on the Physical and Mechanical Properties of the Shell of a High-Pressure Vessel for Hydrogen Storage. *Russ. J. Phys. Chem. B* **2022**, *16*, 1172-1179, https://doi.org/10.1134/S1990793122060070.
23. Troshin, K.Y.; Rubtsov, N.; Tsvetkov, G.; Chernysh, V.; Shamshin, I. Initiation of Hydrogen–Air Mixtures with Metallic Rh and Hydrogen–Methane/Ethane/Ethylene–Air Mixtures with Pd and Rh at Pressures of 1–2 atm. *Russ. J. Phys. Chem. B* **2022**, *16*, 693-698, https://doi.org/10.1134/S1990793122040303.
24. Dokhlikova, N.; Gatin, A.; Sarvadiy, S.Y.; Ozerin, S.; Rudenko, E.; Grishin, M.; Shub, B. Modelling Hydrogen Adsorption on a Copper Nanoparticle Deposited on a Graphite Substrate with Various Defects. *Russ. J. Phys. Chem. B* **2022**, *16*, 772-779, https://doi.org/10.1134/S1990793122040042.

25. Trakhtenberg, L.I. Sensor Layers Based on Semiconductor Nanoparticles and Their Electronic Structure. *Russ. J. Phys. Chem. B.* **2023**, *17*, 600–607,https://doi.org/10.1134/S1990793123030144.
26. Mollaamin, F.; Monajjemi, M. Electric and Magnetic Evaluation of Aluminum–Magnesium Nanoalloy Decorated with Germanium Through Heterocyclic Carbenes Adsorption: A Density Functional Theory Study. *Russ. J. Phys. Chem. B.* **2023**, *17*, 658–672, https://doi.org/10.1134/S1990793123030223.
27. Kucherenko, M.; Neyasov, P.; Kruchinin, N.Y. Modeling Conformational Rearrangements of a Macromolecule Adsorbed on a Metal Nanoparticle in an External Electric Field. *Russ. J. Phys. Chem. B* **2023**, *17*, 745-754, https://link.springer.com/article/10.1134/S1990793123030053.
28. Mollaamin, F.; Monajjemi M. Graphene-based resistant sensor decorated with Mn, Co, Cu for nitric oxide detection: Langmuir adsorption & DFT method. *Sensor Rev.* **2023**, *43*, 266–279, https://doi.org/10.1108/sr-03-2023-0040.
29. Golyak, I.S.; Anfimov, D.; Vintaykin, I.; Golyak, I.S.; Drozdov, M.; Morozov, A.; Svetlichnyi, S.; Tabalin, S.; Timashova, L.; Fufurin, I. Monitoring greenhouse gases in the open atmosphere by the Fourier spectroscopy method. *Russ. J. Phys. Chem. B* **2023**, *17*, 320-328, https://doi.org/10.1134/S1990793123020264.
30. Mollaamin, F.; Monajjemi, M. Tailoring and functionalizing the graphitic-like GaN and GaP nanostructures as selective sensors for NO, NO_2, and NH_3 adsorbing: A DFT study. *J. Mol. Model.* **2023**, *29*, 170, https://doi.org/10.1007/s00894-023-05567-8.
31. Avilova, M.M.; Zolotareva, N.V.; Popova, O.V. Molecular Modeling of the Interaction of a Cluster of Chromium-Containing Polyacrylonitrile with Pollutant Gases. *Russ. J. Phys. Chem. B.* **2023**, *17*, 329–335, https://doi.org/10.1134/S1990793123020203.
32. Mollaamin, F.; Monajjemi, M. Divulge of Hydrogen Energy Storage by Manganese Doped Nitrogen Nanocomposites of Aluminum, Gallium or Indium Nitrides: A First-Principles Study. *Russ. J. Phys. Chem. B.* **2025**, *19*, 319–335, https://doi.org/10.1134/S199079312570006X.
33. Shahriari, S.; Mollaamin, F.; Monajjemi, M. Increasing the Performance of {[(1-x-y) $LiCo_{0.3}Cu_{0.7}$] (Al and Mg doped)] O_2}, xLi_2MnO_3, $yLiCoO_2$ Composites as Cathode Material in Lithium-Ion Battery: Synthesis and Characterization. *Micromachines* **2023**, *14*, 241, https://doi.org/10.3390/mi14020241.
34. Mollaamin, F.; Monajjemi, M. Perspective of Clean Energy-saving by Semiconducting Quantum Dot Nanomaterials through Photoelectric and Density of States Analysis. *J Fluoresc.* **2025**, https://doi.org/10.1007/s10895-025-04207-z.
35. Mollaamin, F. Anchoring of 2D layered materials of $Ge_5Si_5O_{20}$ for (Li/Na/K)-(Rb/Cs) batteries towards Eco-friendly energy storage. *BMC Chemistry.* **2025**, *19*, 233, https://doi.org/10.1186/s13065-025-01593-0.
36. Monajjemi, M.; Mollaamin, F.; Shahriari, S. Khalaj, Z.; Sakhaeinia, H.; Alihosseini, A. Interaction of Nano-Boron Nitride Sheets with Electrodes in Lithium Ion Battery for Increasing Voltage and Amperage. *Russ. J. Phys. Chem. B.* **2024**, *18*, 1090–1112, https://doi.org/10.1134/S1990793124700465.
37. Mollaamin, F. Investigating the Treatment of Transition Metals for Ameliorating the Ability of Boron Nitride for Gas Sensing & Removing: A Molecular Characterization by DFT Framework. *Prot. Met. Phys. Chem. Surf.* **2024**, *60*,1050–1063, https://doi.org/10.1134/S2070205124702502.
38. Mollaamin, F.; Monajjemi, M. Corrosion inhibiting by some organic heterocyclic inhibitors through langmuir adsorption mechanism on the Al-X (X = Mg/Ga/Si) alloy surface: A study of quantum three-layer method of CAM-DFT/ONIOM. *J. Bio- Tribo-Corros.* **2023**, *9*, 33, https://doi.org/10.1007/s40735-023-00751-y.
39. Mollaamin, F.; Monajjemi, M. Structural, Electromagnetic and Thermodynamic Analysis of Ion Pollutants Adsorption in Water by Gallium Nitride Nanomaterial: a Green Chemistry Application. *Russ. J. Phys. Chem. B.* **2024**, *18*, 533–548, https://doi.org/10.1134/S199079312402012X.
40. Mollaamin, F.; Monajjemi, M. An Architectural Battery Designed by Substituting Lithium with Second Main Group Metals (Be, Mg, Ca/Cathode) and Hybrid Oxide of Fourth Group Ones (Si, Ge, Sn/Anode) Nanomaterials Towards H_2 Adsorption: A Computational Study. *Nanomaterials* **2025**, *15*, 959, https://doi.org/10.3390/nano15130959
41. Mollaamin, F.; Monajjemi, M. Molecular Structure Study of Decorated Boron Nitride Systems with Transition Metals (Cr, Ni, Zn, Mo, Pd, Cd) for Boosting Hydrogen Sorption: Nanomaterials Insight into Battery Technology. *Russ. J. Phys. Chem. B.* **2025**, *19*, 1–20, https://doi.org/10.1134/S1990793124701501.
42. Mollaamin, F.; Monajjemi, M.; Mohammadi, S.; Shahriari, S. Modelling and Characterization of Silicon and Germanium Oxides as Nano-Hybrid Materials for Hydrogen Storage in Cell Batteries: a First-Principle Study. *Russ. J. Phys. Chem. B*. **2025**, *19*, 217–235, https://doi.org/10.1134/S1990793124701677.

43. Mollaamin, F. Alkali Metals Doped on Tin-Silicon and Germanium-Silicon Oxides for Energy Storage in Hybrid Biofuel Cells: A First-Principles Study. *Russ. J. Phys. Chem. B.* **2025**, *19*, 722–736, https://doi.org/10.1134/S1990793125700393.
44. Mollaamin, F.; Monajjemi, M. Unraveling Hetero-Clusters of Indium Gallium Nitride and Its Alloys for Solar Cells Development: Structural and Characterization Study of Nitride-Based Semiconductors Using DFT Framework. *Russ. J. Phys. Chem. B* **2025**, *19*, 480–500, https://doi.org/10.1134/S1990793125700174.
45. Mollaamin, F.; Monajjemi, M. Effect of Implanted Titanium, Vanadium or Chromium on Boron Nitride Surface for Increasing Carbon Monoxide Adsorption: Designing Gas Sensor for Green Chemistry Future. *Russ. J. Phys. Chem. B* **2024**, *18*, 1199–1216, https://doi.org/10.1134/S1990793124700519.
46. Monajjemi, M.; Mollaamin, F.; Shahriari, S.; Mohammadi, S. Synthesis of Nano C60-[Fe_3O_4/SiO_2/GeO_2] as Efficient Catalyst Disinfection. *Russ. J. Phys. Chem. B.* **2024**, *18*, 1217–1225, https://doi.org/10.1134/S1990793124700349.
47. Mollaamin, F.; Computational Methods in the Drug Delivery of Carbon Nanocarriers onto Several Compounds in Sarraceniaceae Medicinal Plant as Monkeypox Therapy. *Computation* **2023**, *11*, 84, https://doi.org/10.3390/computation11040084
48. Davtyan, A.H.; Manukyan, Z.O.; Arsentev, S.D.; Tavadyan, L.A.; Arutyunov, V.S. Investigation of Potential Energy Surfaces of Reaction Systems Containing Ethylene, Hydrogen, and Oxygen Atoms by Quantum Chemical Calculations. *Russ. J. Phys. Chem. B* **2023**, *17*, 336–345, https://doi.org/10.1134/S1990793123020239.
49. Troshin, K.Y.; Rubtsov, N.M.; Tsvetkov, G.I.; Chernysh, V.I.; Shamshin, I.O. Ignition Limits of Hydrogen–Methane–Air Mixtures Over Metallic Rhodium at a Pressure of up to 2 atm. *Russ. J. Phys. Chem. B* **2023**, *17*, 433–438, https://doi.org/10.1134/S1990793123020185.
50. Mollaamin, F.; Monajjemi M. In Silico-DFT investigation of nanocluster alloys of Al-(Mg, Ge, Sn) coated by nitrogen heterocyclic carbenes as corrosion inhibitors. *J. Clust. Sci.* **2023**, *34*, 2901–2918, https://doi.org/10.1007/s10876-023-02436-5.
51. Mollaamin, F.; Monajjemi, M. Transition metal (X = Mn, Fe, Co, Ni, Cu, Zn)-doped graphene as gas sensor for CO_2 and NO_2 detection: A molecular modeling framework by DFT perspective. *J. Mol. Model.* **2023**, *29*,119, https://doi.org/10.1007/s00894-023-05526-3.
52. Perdew, J.P.; Burke, K.; Ernzerhof, M. Generalized Gradient Approximation Made Simple. *Phys. Rev. Lett.* **1996**, *77*, 3865, https://doi.org/10.1103/PhysRevLett.77.3865.
53. Alaya, R.; Kourchid, K.; Althaqafi, Y.; Mbarki, M.; Rebey, A. Structural, Electronic and Optical Properties of the Ordered InP1–xBi x: An Ab-Initio Study. *Russ. J. Phys. Chem. B* **2023**, *17*, 868-877, https://doi.org/10.1134/S1990793123040024.
54. Yuan, X.; Tan, X.; Liu, B. Structural, Mechanical, Electronic and Optical Properties of Spinel $ZnAl_2O_4$ Underpressure from First-Principles Calculations. *Russ. J. Phys. Chem. B* **2023**, *17*, 886–895, https://doi.org/10.1134/S1990793123040322.
55. Hohenberg, P.; Kohn, W. Inhomogeneous Electron Gas. *Phys. Rev. B* **1964**, *136*, B864–B871, https://doi.org/10.1103/PhysRev.136.B864.
56. Kohn, W.; Sham, L.J. Self-Consistent Equations Including Exchange and Correlation Effects. *Phys. Rev.* **1965**, *140*, A1133–A1138, https://doi.org/10.1103/PhysRev.140.A1133.
57. Becke, A.D. Density-functional thermochemistry. III. The role of exact exchange. *J. Chem. Phys.* **1993**, *98*, 5648–5652, https://doi.org/10.1063/1.464913.
58. Lee, C.; Yang,W.; Parr, R.G.Development of the Colle–Salvetti correlation-energy formula into a functional of the electron density. *Phys. Rev. B* **1988**, *37*, 785–789, https://doi.org/10.1103/PhysRevB.37.785.
59. Mollaamin, F.; Monajjemi, M. In Situ Ti-Embedded SiC as Chemiresistive Nanosensor for Safety Monitoring of CO, CO_2, NO, NO_2: Molecular Modelling by Conceptual Density Functional Theory. *Russ. J. Phys. Chem. B* **2024**, *18*, 49–66, https://doi.org/10.1134/S1990793124010159.
60. Stephens, P.J.; Devlin, F.J.; Chabalowski, C.F.; Frisch, M.J. Ab initio calculation of vibrational absorption and circular dichroism spectra using density functional force fields. . *Phys. Chem.* **1994**, *98*, 11623-11627, https://doi.org/10.1021/j100096a001.
61. Mollaamin, F.; Monajjemi, M. Fractal dimension on carbon nanotube-polymer composite materials using percolation theory. *J. Comput. Theor. Nanosci.* **2012**, *9*, 597–601, https://doi.org/10.1166/jctn.2012.2067.
62. Mollaamin, F.; Monajjemi, M. Adsorption ability of Ga_5N_{10} nanomaterial for removing metal ions contamination from drinking water by DFT. *Int. J. Quantum Chem.* **2024**, *124*, e27348, https://doi.org/10.1002/qua.27348.

63. Mollaamin, F.; Monajjemi, M. Molecular modelling framework of metal-organic clusters for conserving surfaces: Langmuir sorption through the TD-DFT/ONIOM approach. *Mol. Simul.* **2022**, *49*, 365–376, https://doi.org/10.1080/08927022.2022.2159996.
64. Touhami, H.; Almi, K.; Lakel, S.; Boumezrag, M. Alkali Doping Nickel Oxide Thin Films Using Sol-Gel Spin Coated and Density Functional Theory: Structural and Physical Properties. *Russ. J. Phys. Chem. B* **2023**, *17*, 1057-1068, https://doi.org/10.1134/S1990793123050287.
65. Frisch, M.J.; Trucks, G.W.; Schlegel, H.B.; Scuseria, G.E.; Robb, M.A.; Cheeseman, J.R.; Scalmani, G.; Barone, V.; Petersson, G.A.; Nakatsuji, H.; Li, X.; Caricato, M.; Marenich, A.V.; Bloino, J.; Janesko, B.G.; Gomperts, R.; Mennucci, B.; Hratchian, H.P.; Ortiz, J. V.; Izmaylov, A. F.; Sonnenberg, J.L.; Williams-Young, D.; Ding, F.; Lipparini, F.; Egidi, F.; Goings, J.; Peng, B.; Petrone, A.; Henderson, T.; Ranasinghe, D.; Zakrzewski, V.G.; Gao, J.; Rega, N.; Zheng, G.; Liang, W.; Hada, M.; Ehara, M.; Toyota, K.; Fukuda, R.; Hasegawa, J.; Ishida, M.; Nakajima, T.; Honda, Y.; Kitao, O.; Nakai, H.; Vreven, T.; Throssell, K.; Montgomery, J.A., Jr.; Peralta, J.E.; Ogliaro, F.; Bearpark, M.J.; Heyd, J.J.; Brothers, E.N.; Kudin, K.N.; Staroverov, V.N.; Keith, T.A.; Kobayashi, R.; Normand, J.; Raghavachari, K.; Rendell, A.P.; Burant, J.C.; Iyengar, S.S.; Tomasi, J.; Cossi, M.; Millam, J.M.; Klene, M.; Adamo, C.; Cammi, R.; Ochterski, J.W.; Martin, R.L.; Morokuma, K.; Farkas, O.; Foresman, J.B.; Fox, D.J. Gaussian 16, Revision C.01, Gaussian, Inc., Wallingford CT, **2016**.
66. Dennington, R.; Keith Todd, A.; Millam John, M. GaussView, Version 6.06.16. Semichem Inc., Shawnee Mission, KS, USA, **2016**.
67. Mollaamin, F.; Monajjemi, M. Application of DFT and TD-DFT on Langmuir Adsorption of Nitrogen and Sulfur Heterocycle Dopants on an Aluminum Surface Decorated with Magnesium and Silicon. *Computation* **2023**, *11*, 108, https://doi.org/10.3390/computation11060108.
68. Mollaamin, F.; Monajjemi, M. Doping of graphene nanostructure with Iron, Nickel and Zinc as selective detector for the toxic gas removal: A density functional theory study. *C–Journl of Carbon Research.* **2023**, *9*, 20, https://doi.org/10.3390/c9010020.
69. Mollaamin, F.; Mohammadi, S.; Khalaj, Z.; Monajjemi, M. Computational Modelling of Boron Nitride Nanosheet for Detecting and Trapping of Water Contaminant. *Russ. J. Phys. Chem. B* **2024**, *18*, 67–82, https://doi.org/10.1134/S1990793124010330.
70. Shmyreva, A.; Kirillov, V.; Dzhangurazov, E.; Yurkov, G.Y. Inhomogeneous Magnetic Structure of the Metallic FM Part of Co/CoO Nanoparticles by the 59Co Nuclear Magnteic Resonance Method. *Russ. J. Phys. Chem. B* **2023**, *17*, 764-773, https://doi.org/10.1134/S1990793123030120.
71. Mollaamin, F.; Shahriari, S.; Monajjemi, M.; Khalaj, Z. Nanocluster of Aluminum lattice via organic inhibitors coating: A study of freundlich adsorption. *J. Clust. Sci.* **2023**, *34*, 1547–1562, https://doi.org/10.1007/s10876-022-02335-1.
72. Li, W.; Wang, S.; Jiang, L.; Jiang, W.; Wu, Y.; Guo, X.; Yuan, H.; Luo, M. Hydrogen Storage Performance of Doped Hexagonal Boron Nitride Nanosheets with Thin Layers. *Langmuir* **2025**, *41*, 4471–4481, https://doi.org/10.1021/acs.langmuir.4c03682.

Publisher's Note & Disclaimer